Vol 14 No 10, October 2005
1009-1963/2005/14(10)/1966-08

Chinese Physics

© 2005 Chin. Phys. Soc.
and IOP Publishing Ltd

Experimental and calculated momentum densities for the complete valence orbitals of the antimicrobial agent diacetyl*

Su Guo-Lin(苏国林), Ren Xue-Guang(任雪光), Zhang Shu-Feng(张书锋), Ning Chuan-Gang(宁传刚), Zhou Hui(周 晖), Li Bin(李 彬), Li Gui-Qin(李桂琴), and Deng Jing-Kang(邓景康)†

Department of Physics, Key Laboratory of Atomic and Molecular NanoSciences, Ministry of Education, Tsinghua University, Beijing 100084, *China*

(Received 10 May 2005; revised manuscript received 30 May 2005)

The first electronic structural study of the complete valence shell binding energy spectra of the antimicrobial agent diacetyl, encompassing both the outer and inner valence regions, is reported. The binding energy spectra as well as the individual orbital momentum profiles have been measured by using a high resolution (e, 2e) electron momentum spectrometer (EMS) at an impact energy of 1200eV plus the binding energy, and using symmetric noncoplanar kinematics. The experimental orbital electron momentum profiles are compared with self-consistent field (SCF) theoretical profiles calculated using the Hartree–Fock approximation and Density Functional theory predictions in the target Kohn-Sham approximation which includes some treatment of correlation via the exchange and correlation potentials with a range of basis sets. The pole strengths of the main ionization peaks from the inner valence orbitals are estimated.

Keywords: diacetyl, ionization energy, electron momentum profiles, electron correlation effects
PACC: 3480D, 3480G

1. Introduction

Since the pioneer researches by Amaldi *et al.*[1] and Weigold *et al*,[2] electron momentum spectroscopy (EMS) with symmetric non-coplanar geometry based on a binary (e, 2e) ionization reaction, which provides unique and detailed information on the electronic structures of atoms and molecules,[3−10] has developed rapidly. The technique can have access to the complete valance shell binding energy range, though with lower resolution than that in most photoelectron spectroscopy (PES) studies, and the orbital density imaging information provided by EMS momentum profiles is unique. Now it has become practical to apply EMS to studies of larger molecules of biological and pharmaceutical interest.[7,11−13] In particular, EMS measurements of the momentum profiles for individual orbitals in atoms and molecules have taken significant improvements in theoretical quantum chemistry in computing electron correlation effects (i.e. developments of generalized gradient approximations in density function theory (DFT)), to permit measurements on larger molecules together with meaningful interpretation of the results. The extension of EMS to biomolecules and pharmaceuticals is particularly appealing because of possible applications in experimental testing, validation and evaluation of computational chemical methods used for computer-aided drug design and the prediction of reactivity. Several EMS studies of biologically important larger molecules such as the aminoacid glycine[7,11] and urotropine[14] have been reported together with quantum chemical calculations using HF and DFT methods.

Diacetyl, as is known as 2, 3-butanedione, has received much attention because of the antimicrobial activity against Escherichia coli, Listeria monocytogenes and Staphylococcus aureus.[15] It has been widely studied by photoelectron spectroscopy (PES)[16,17] and also analysed by two new spectrophotometric and

*Project supported by the National Natural Science Foundation of China (Grant Nos 19854002, 19774037 and 10274040) and the Research Fund for the Doctoral Program Foundation of Institution of Higher Education of China (Grant No 1999000327).
†E-mail: djk-dmp@mail.tsinghua.edu.cn

fluorimetric methods in yogurt.[18] In this paper, the complete valence binding energy spectra and electron momentum profiles for the complete valence orbitals of diacetyl are presented. The experimental momentum profiles are compared with HF and DFT calculations using various basis sets.

2. Experimental method and theoretical background

An energy-dispersive multichannel electron momentum spectrometer with a symmetric non-coplanar geometry was used in this work. The details of the spectrometer constructed at Tsinghua University have been reported previously.[19] In the EMS experiment the relative (e, 2e) cross section for electron impact ionization (i.e. the binary (e, 2e) reaction) is measured by detecting the two outgoing electrons (scattered and ionized) in coincidence. A newly developed multiparameter data acquisition system based on universal serial bus (USB) interface was used for data acquisition and experimental controls in this spectrometer.[20] The particular kinematics of the experiment is chosen in such a way as to provide a straightforward relation between some variable kinematic parameters and the momentum of the ionized electron prior to knock-out. For this purpose the symmetric non-coplanar kinematics[3] is the most convenient and frequently used in experimental configuration.

In the symmetric non-coplanar scattering geometry, the two outgoing electrons are selected to have equal polar angles ($\theta_1 = \theta_2 = 45°$) relative to the direction of incident electron beam. The relative azimuthal angle ϕ between the directions of two outgoing electrons is varied by rotating one of the analysers over the range from 0° to ±30° around the incident beam axis. Under conditions of high impact energy and high momentum transfer, the target electron essentially undergoes a clean "knock-out" collision. In this situation several approximations, of which the most important are the binary encounter approximation and the plane wave impulse approximation (PWIA), provide a very good description of the collision. In the PWIA, the momentum p of the electron prior to knock-out is related to the azimuthal angle by[3]

$$p = [(2p_1 \cos\theta_1 - p_0)^2 + (2p_1 \sin\theta_1 \sin(\phi/2))^2]^{1/2}, \quad (1)$$

where $p_1 = p_2 = \sqrt{2E_1}$ is the magnitude of the momentum of each outgoing electron and $p_0 = \sqrt{2E_0}$ is the momentum of the incident electron (both in atomic units). Under these conditions the kinematic factors are effectively constant,[3] the EMS cross section for randomly oriented gas-phase targets, σ_{EMS}, can be given by

$$\sigma_{\mathrm{EMS}} \propto S_{\mathrm{f}}^2 \int \mathrm{d}\Omega |\langle p\, \Psi_{\mathrm{f}}^{N-1} | \Psi_{\mathrm{i}}^{N} \rangle|^2, \quad (2)$$

where p is the momentum of the target electron prior to ionization and S_{f}^2 is pole strength. $\left|\Psi_{\mathrm{f}}^{N-1}\right\rangle$ and $\left|\Psi_{\mathrm{i}}^{N}\right\rangle$ are the total electronic wavefunctions for the final ion state and the target molecule ground (initial) state, respectively. The $\int \mathrm{d}\Omega$ represents the spherical average due to the randomly oriented gas phase target. The overlap of the ion and neutral wavefunctions in Eq.(2) is known as the Dyson orbital while the square of this quantity is referred to as an ion-neutral overlap distribution (OVD). Thus, the (e, 2e) cross section is essentially proportional to the spherical average of the square of the Dyson orbital in momentum space.

Equation (2) is greatly simplified by using the Target Hartree–Fock approximation (THFA). Within the THFA, only final (ion) state correlation is allowed and the many-body wavefunctions $\left|\Psi_{\mathrm{f}}^{N-1}\right\rangle$ and $\left|\Psi_{\mathrm{i}}^{N}\right\rangle$ are approximated as independent particle determinants of ground state target Hartree–Fock orbitals. In this approximation Eq.(2) reduces to

$$\sigma_{\mathrm{EMS}} \propto S_j^{\mathrm{f}} \int \mathrm{d}\Omega\, |\psi_j(p)|^2, \quad (3)$$

where $\psi_j(p)$ is the one-electron momentum space canonical Hartree–Fock orbital wavefunction for the jth electron, corresponding to the orbital from which the electron is ionized, S_j^{f} is the spectroscopic factor, the probability of the ionization event producing a one-hole configuration of the final ion state. The integral in Eq.(3) is known as the spherically averaged one-electron momentum distribution. To this extent EMS has the ability to image the electron density in individual "orbitals" selected according to their binding energies.

Equation (2) has recently been re-interpreted[21] in the context of Kohn-Sham density functional theory (DFT) and the Target Kohn-Sham Approximation (TKSA) gives a result similar to that from Eq.(3) but with the canonical Hartree–Fock orbital replaced by a momentum space Kohn-Sham orbital $\psi_j^{\mathrm{KS}}(p)$,

$$\sigma_{\mathrm{EMS}} \propto \int \mathrm{d}\Omega |\, \Psi_j^{\mathrm{KS}}(p)|^2. \quad (4)$$

It should be noted that the accounting of electron correlation effects in the target ground state is

included in the TKSA via the exchange correlation potential. A more detailed description of the TKSA-DFT method may be found elsewhere.[21]

3. Calculations

In the present work, spherically averaged theoretical momentum profiles have been calculated for the complete valence orbitals of diacetyl using the PWIA. The calculation methods and basis sets are described briefly below. The total number of contracted Gaussian-type orbital functions (CGTO) is also given for each calculation below. The Hartree–Fock and DFT calculations are carried out using the Gaussian 98 program.[22] The Hartree–Fock calculations of the momentum profiles are performed by using Eq.(3) with the basis sets of STO-3G, 6-31G and 6-311++G**. The B3LYP functionals are used for the DFT calculations. Two basis sets of 6-31G and 6-311++G** are used for the DFT calculations.

1) STO-3G: A minimal basis set, being effectively of single zeta quality, using a single contraction of three Gaussian functions for each basis function. Thus each function consists of C(6s,3p)/[2s,1p], O(6s,3p)/[2s,1p] and H(3s)/[1s] contractions. Therefore, a total of 36 CGTO are employed for diacetyl. This basis set was designed by Pople and coworkers.[23]

2) 6-31G: The 6-31G basis comprises of an inner valence shell of six s-type Gaussians and an outer valence shell which has been split into two parts represented by three and one primitives. Both carbon and oxygen atoms have a (10s, 4p)/[3s,2p] contraction and hydrogen atoms have a (4s)/[2s] contraction. A total of 66 CGTO are used for diacetyl. A detailed description of this basis set developed by Pople and co-workers can be found in Ref.[24].

3) 6-311++G**: The 6-311++G** is an augmented version by Pople *et al.* The outer valence shell is split into three parts and represented by three, one and one primitives. Based on the 6-311G basis very diffused s- and p-functions are added to both carbon and oxygen atoms and diffuse s-function are added to hydrogen atoms.[24–26] In addition, polarization functions are also included in the basis, a single set of five d-type Gaussian functions for C and O atoms and a single set of uncontracted p-type Gaussian functions for H atoms. Thus a (12s, 6p, 1d) contracts to [5s, 4p, 1d] for C and O atoms, and a (6s, 1p) to [4s, 1p] for H atoms. The number of CGTO is 174 for diacetyl.

The geometry of diacetyl reported by Hagen and Hedberg[27] has been used for all calculations. In order to compare the calculated cross-sections with the experimental electron momentum profiles the effects of the finite spectrometer acceptance angles in both θ and ϕ ($\Delta\theta = \pm 0.6^\circ$ and $\Delta\theta = \pm 1.2^\circ$) are included using the Gaussian-weighted planar grid (GW-PG) method.[28]

4. Results and discussion

Diacetyl contains 46 electrons and has C_{2h} symmetry point group. According to molecular orbital theory, the ground state electronic configuration can be written as

$$(\text{core})^{12}\underbrace{(4a_g)^2(4b_u)^2(5a_g)^2(5b_u)^2(6a_g)^2}_{\text{inner valence}},$$

$$\underbrace{(6b_u)^2(7a_g)^2(1a_u)^2(7b_u)^2(1b_g)^2(8a_g)^2(8b_u)^2(9a_g)^2(2a_u)^2(2b_g)^2(9b_u)^2(10a_g)^2}_{\text{Outer valence}}.$$

The valence-shell contains seventeen molecular orbitals and can be divided into two sets of five inner valence and twelve outer valence orbitals. The order of these valence orbitals has been established, by both PES and molecular calculations.[17]

4.1. Binding energy spectra

In order to obtain the experimental momentum profiles, twelve binding energy spectra over an energy range of 1–40eV are collected at the out-of-plane azimuth angles ϕ= 0°, 1°, 2°, 3°, 4°, 5°, 7°, 10°, 12°, 14°, 17° and 22° in a series of sequential repetitive scans. Figure 1 shows the binding energy spectra of diacetyl in the range 1–40eV for measurements at summed all ϕ angles at an incident energy of 1200eV plus the binding energy. The spectra in Fig.1 are fitted with a set of individual Gaussian peaks. The fitted Gaussians for individual peaks are indicated by dashed lines while their sum, i.e. the overall fitted spectra, are represented by the solid lines. Except for the last peak at 32.7eV, the widths of the peaks are combinations of the EMS instrumental energy resolution and the cor-

responding Franck–Condon widths derived from high resolution PES data,[17] and the relative energy values of the peaks are given by the relative ionization energies determined by high resolution PES. The ionization potential value and the width of the last peak are determined by our EMS experiment. The differences in FWHM between the orbitals are due to the vibrational broadening of the lines.

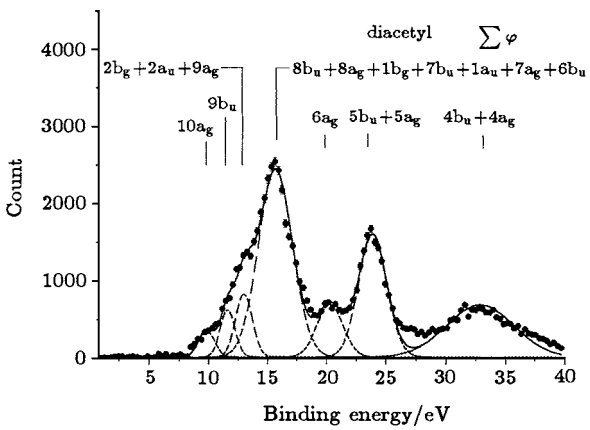


Fig.1. Valence shell binding energy spectra of 1200eV for diacetyl at summed all ϕ angles. The dashed and solid lines represent individual and summed Gaussian fits respectively.

The PES spectra of the twelve outer valence and three inner valence region have been reported by Niessen *et al.*[17] In the work, the vertical ionization potentials of the $10a_g$ and $9b_u$ orbitals were determined to be 9.6 and 11.5eV, respectively. However, the three orbitals, $2b_g$, $2a_u$ and $9a_g$, whose vertical ionization potentials were from 12.6 to 14.0eV, were not well resolved. The same is true of the next three orbitals, $8b_u$, $8a_g$ and $1b_g$, with the vertical ionization potentials from 14.5 to 15.2eV. In sequence, 16.0, 16.0, 16.5, 17.4, 20.6, 24.0 and 24.0eV were respectively assigned to the vertical ionization potentials of the $7b_u$, $1a_u$, $7a_g$, $6b_u$, $6a_g$, $5b_u$ and $5a_g$ orbitals.

In the EMS binding energy spectra in Fig.1, however, only seven structures can be well identified. The vertical ionization potentials of the two outer valence orbitals, $10a_g$ and $9b_u$ are at 9.6 and 11.4eV respectively. The average vertical ionization potentials of the ($2b_g+2a_u$ + $9a_g$) and ($8b_u+8a_g+$ $1b_g+7b_u+1a_u+7a_g$ $+6b_u$) outer valence orbital sums are determined to be 12.8 and 15.8eV, respectively. The band located at 20.4eV corresponds to the removal of an electron from the $6a_g$ inner valence orbital. In sequence, 23.8 and 32.7eV are assigned to the average vertical ionization potentials of ($5b_u+5a_g$) and ($4b_u$ + $4a_g$) inner valence orbital sums respectively. It should also be noted that no results before have been reported for the ionization potential values of the $4b_u$ and $4a_g$ orbitals as far as we know, although our EMS experiment could not resolve the two orbitals due to the insufficient resolution of the EMS.

4.2. Experimental and theoretical momentum distributions

Experimental momentum profiles (XMPs) have been extracted by deconvolution of the sequentially obtained angular-correlated binding energy spectra, and therefore the relative normalization for the different transitions is maintained. For all orbitals, the various theoretical momentum profiles (TMPs) are obtained with the methods described in Section 2, and the experimental instrumental angular resolutions have been incorporated in the calculations using the UBC RESFOLD program based on the GW-PG method.[26] Experimental data and theoretical values have been placed on a common intensity scale by normalizing the experimental to the DFT-B3LYP/6-311++G** theoretical momentum profile for the $10a_g$ orbital, and the relative normalization is preserved for all other orbitals.

The theoretical and experimental momentum profiles of the complete valence shell orbitals of diacetyl are presented in Figs.2–8. In the following discussion the comparisons between the theoretical calculations and the experimental data are provided for the outer valence orbitals and inner valence orbitals in turn.

The electron density of the HOMO plays an important role in determining the chemical reactivity as indicated by the frontier molecular orbital theory of Fukui[29] and the work of Woodward and Hoffman.[30] Therefore it is important to obtain a detailed understanding of the electronic structure of the HOMO. The currently determined experimental momentum profile for the $10a_g$ HOMO of diacetyl is shown in Fig.2, together with the theoretical momentum profiles calculated using HF and DFT/B3LYP methods employing the STO-3G, 6-31G and 6-311++G** basis sets. This orbital has a "s-p type" momentum distribution character as shown in Fig.2. In the momentum range above about 0.1 a.u., it can be seen that, except for HF/STO-3G (curve 5), the calculated theoretical momentum profiles provide a good agreement with the experimental profile, whereas, the HF/STO-3G calculation seems to be consistent with the first experimental point near the zero momentum.

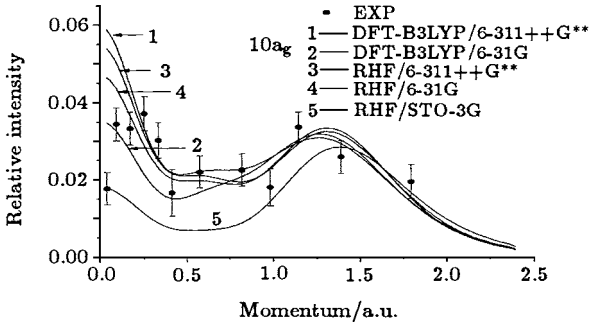


Fig.2. Experimental and calculated momentum distributions for the HOMO $10a_g$ of diacetyl. The TMPs are calculated by using DFT-B3LYP (curves 1 and 2) method with the 6-311++G** and 6-31G basis sets and Hartree–Fock method (curves 3, 4 and 5) with the 6-311++G**, 6-31G and STO-3G basis sets.

Experimental and theoretical momentum profiles for the $9b_u$ orbital are shown in Fig.3. The experimental and the theoretical momentum profiles show the expected "p–p type" distribution. In the momentum range above about 0.7 a.u., it can be seen that, except for HF/STO-3G (curve 5), the calculated theoretical momentum profiles are very similar and fit to the experimental momentum profile very well. However, the intensities of the five calculated theoretical momentum profiles are quite different in the low momentum range, thus the experimental distribution acts as a criterion for evaluating the quality of quantum chemical calculations. It can be seen from Fig.3 that the calculation of HF method with 6-311++G** basis set (curve 3) gives a better description of the experimental momentum profile in both the shape and the intensity in the low momentum region than other calculations.

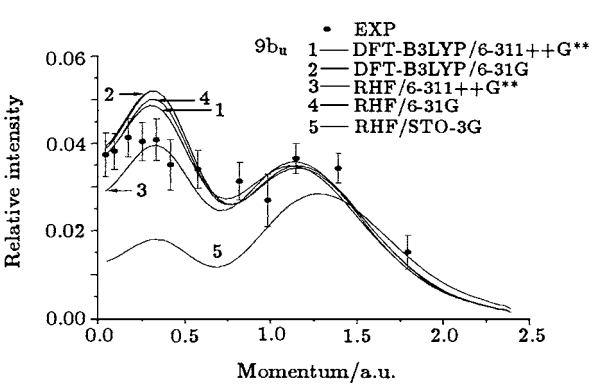


Fig.3. Experimental and calculated momentum distributions for the $9b_u$ of diacetyl. The TMPs are calculated by using DFT-B3LYP (curves 1 and 2) method with the 6-311++G** and 6-31G basis sets and Hartree–Fock method (curves 3, 4 and 5) with the 6-311++G**, 6-31G and STO-3G basis sets.

Whereas, the calculations of DFT/B3LYP method employing the 6-311++G** and 6-31G basis sets (curves 1 and 2) and HF method with 6-31G basis set (curve 4) overestimate the intensity of the experimental profile, and the calculation of HF/STO-3G (curve 5) gives the worst fit of the experimental distribution in the low momentum range.

The third peak of diacetyl corresponds to $2b_g$, $2a_u$ and $9a_g$ ionizations, which are too close to be separately resolved. In Fig.4, the summed experimental momentum distribution is shown together with the theoretical momentum distributions (curves 1–5) calculated using HF and DFT/B3LYP methods with various basis sets. In the momentum range above 0.2 a.u., it can be seen that, except for HF/STO-3G (curve 5), the calculated theoretical momentum profiles provide a good agreement with the experimental profile. Whereas, all calculated theoretical momentum profiles underestimate the observed intensity of the experimental momentum profile in the low momentum region. The discrepancy between experiment and theory is probably due to inaccuracies in the Gaussian fitting procedures since these orbitals are not well separated and the nearby peak, i.e. $8b_u + 8a_g + 1b_g + 7b_u + 1a_u + 7a_g + 6b_u$ peak is large and could leak into the $2b_g + 2a_u + 9a_g$ peak in the low momentum range. Another possible source for the discrepancy in the low momentum range could be because of the distorted wave effects since the $2b_g$ orbital of diacetyl is a π^*-like molecular orbital. It has been found [31–32] that such orbitals usually produce a "turn-up" of the cross-section in the low momentum range, and this behaviour is similar to the low-p effect observed in atomic d-orbital XMPs. This situation is also probably the case for the $2b_g$ orbital of diacetyl. Such effects in atoms are attributed to distorted wave effects that increase the calculated cross-sections at low-p as observed in the experimental measurements.[31] Similar behaviour has been seen in the XMPs of transition-metal hexacarbonyl HOMOs that are known to be largely metal nd in character.[33] The corresponding transition-metal atoms show such a behaviour, and this is found to decrease with increase of impact energy[33] in the distorted wave impulse approximation (DWIA) calculations. Unfortunately, at present, DWIA calculations are possible only for atoms but not for molecules due to the multicentre nature of the latter.

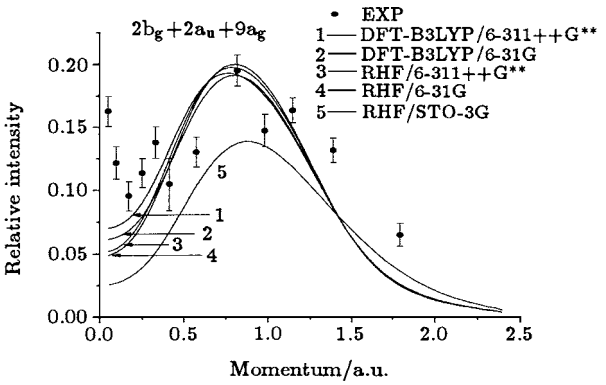


Fig.4. Experimental and calculated spherically averaged momentum distributions for the summed orbitals of the $2b_g$, $2a_u$ and $9a_g$ orbitals of diacetyl. The TMPs are calculated by using DFT-B3LYP (curves 1 and 2) method with the 6-311++G** and 6-31G basis sets and Hartree–Fock method (curves 3, 4 and 5) with the 6-311++G**, 6-31G and STO-3G basis sets.

The fourth peak of diacetyl corresponds to $8b_u$, $8a_g$, $1b_g$, $7b_u$, $1a_u$, $7a_g$ and $6b_u$ ionizations, which are also too close to be separately resolved. In Fig. 5, the summed experimental momentum distribution is shown together with the theoretical momentum distributions calculated using HF and DFT/B3LYP methods with various basis sets. In the momentum range above 0.75 a.u., it can be seen that all theoretical momentum profiles (curves 1–5) provide a good agreement with the experimental profile. But, a comparison of the summed XMPs with various calculations in Fig.5 shows that there is a significant discrepancy between experiment and theory in the low momentum

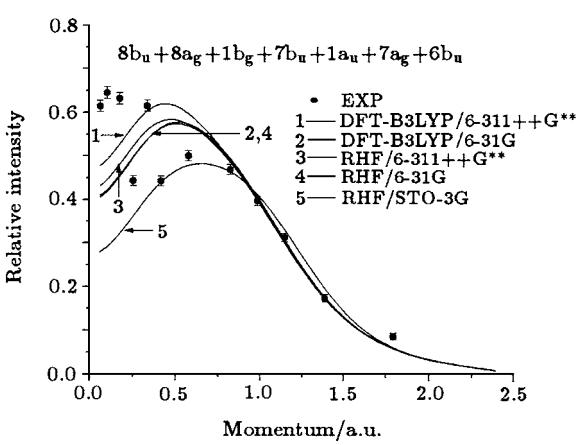


Fig.5. Experimental and calculated spherically averaged momentum distributions for the summed orbitals of the $8b_u$, $8a_g$, $1b_g$, $7b_u$, $1a_u$, $7a_g$ and $6b_u$ orbitals of diacetyl. The TMPs are calculated by using DFT-B3LYP (curves 1 and 2) method with the 6-311++G** and 6-31G basis sets and Hartree–Fock method (curves 3, 4 and 5) with the 6-311++G**, 6-31G and STO-3G basis sets.

range. The discrepancy between experiment and theory is probably due to inaccuracies in the Gaussian fitting procedures since there are seven orbitals in the peak and these orbitals are not well separated. Another possible source for the discrepancy in the low momentum range could be because that outer valence orbitals are very diffuse in position space and thus their diffuse outer regions are possibly difficult to be well modelled by the SCF and DFT variational calculations.

The experimental momentum distribution of the $6a_g$ inner valence orbital is compared in Fig.6 with the five theoretical momentum profiles calculated using DFT-B3LYP (curves 1 and 2) method with the 6-311++G** and 6-31G basis sets, and Hartree–Fock method (curves 3, 4 and 5) with the 6-311++G**, 6-31G and STO-3G basis sets. It can be seen that all five calculations using the DFT and HF methods well reproduce the XMP in high momentum region above 0.5 a.u.. But the calculation results (curves 1, 3 and 4), in particular the Hartree–Fock method with the 6-311++G** basis (curve 3), slightly overestimate the observed intensity in the low momentum range near the zero momentum.

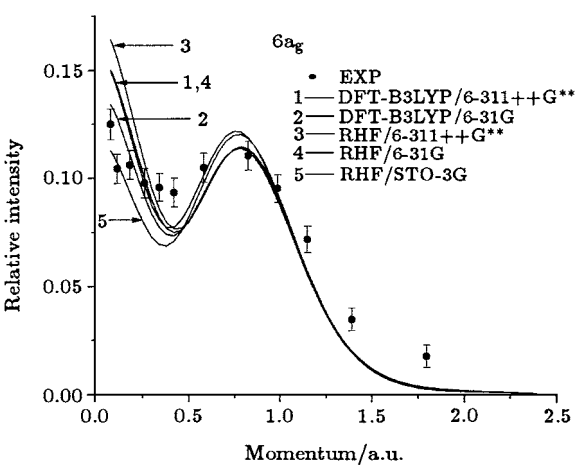


Fig.6. Experimental and calculated momentum distributions for the $6a_g$ of diacetyl. The TMPs are calculated by using DFT-B3LYP (curves 1 and 2) method with the 6-311++G** and 6-31G basis sets and Hartree–Fock method (curves 3, 4 and 5) with the 6-311++G**, 6-31G and STO-3G basis sets.

The sixth peak of diacetyl corresponds to $5b_u$ and $5a_g$ ionizations, which are also too close to be separately resolved. In Fig.7, the summed experimental momentum distribution is shown together with the theoretical momentum distributions calculated using HF and DFT/B3LYP methods with various basis sets. The summed experimental momentum dis-

tribution has a "p-type" character as shown in Fig.7 and it could also be seen that, except for HF/STO-3G (curve 5), the theoretical results are very similar. A comparison between the experimental data and theoretical calculations in Fig.7 shows that all five calculations significantly overestimate the experimental intensity. This indicates that some of the transition intensities from this orbital is located in the higher binding energy range due to the final state electron correlation effects. In order to compare the shape of the momentum distribution, the DFT-B3LYP/6-311++G** calculation (curve 1) is multiplied by an estimated pole strength of 0.59, and the reproduced momentum profile is represented by curve 6 in Fig. 7. Then the experimental result is well described by the DFT-B3LYP/6-311++G** calculation, particulary in the momentum range below 0.75 a.u.. The discrepancy between experiment and theory in the momentum range above 0.75 a.u. is probably due to the distorted wave effects.

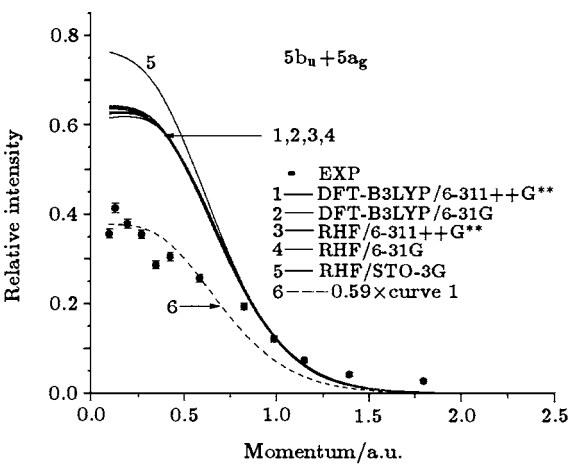


Fig.7. Experimental and calculated spherically averaged momentum distributions for the summed inner valence orbitals of the $5b_u$ and $5a_g$ orbitals of diacetyl. The TMPs are calculated by using DFT-B3LYP (curves 1 and 2) method with the 6-311++G** and 6-31G basis sets and Hartree–Fock method (curves 3, 4 and 5) with the 6-311++G**, 6-31G and STO-3G basis sets. The curve 6 is due to the curve 1 multiplied by an estimated pole strength of 0.59.

The last peak in the inner valence region of the EMS binding energy spectra in Fig.1 is mainly due to the ionizations of the $4b_u$ and $4a_g$ orbitals. The calculated summed momentum distributions for the $4b_u$ and $4a_g$ orbitals are compared with the experimental data in Fig.8. It is obvious that all the five calculations overestimate the experimental intensity. From the above-mentioned discussion about the $5b_u$ and $5a_g$ orbitals, it should also be noted that this energy range around 32 eV may include some intensities from the $5b_u$ and $5a_g$ orbitals. Therefore, estimated spectroscopic factors of 0.50 and 0.30 are used to multiply the DFT-B3LYP calculation with 6-311++G** basis set for the $(4b_u + 4a_g)$ orbitals and the $(5b_u + 5a_g)$ orbitals, respectively, and the summed theoretical curve, represented by the curve 6 in Fig.8, is then compared with the XMP. With the above shape matching scaling factors it can be seen in Fig.8 that a good fit to experimental data is obtained.

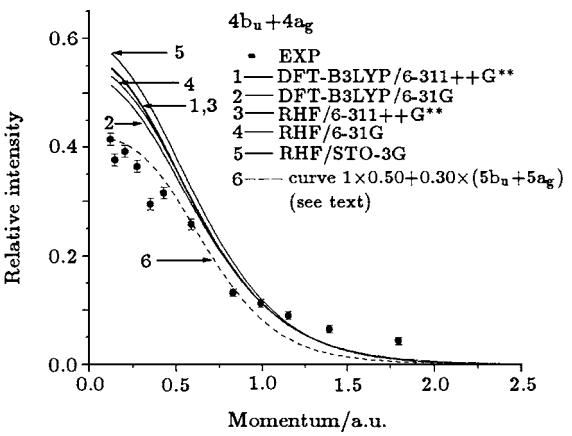


Fig.8. Experimental and calculated spherically averaged momentum distributions for the summed inner valence orbitals of the $4b_u$ and $4a_g$ orbitals of diacetyl. The TMPs are calculated by using DFT-B3LYP (curves 1 and 2) method with the 6-311++G** and 6-31G basis sets and Hartree–Fock method (curves 3, 4 and 5) with the 6-311++G**, 6-31G and STO-3G basis sets. The curve 6 represents a sum of 0.50 × curve 1 of the $4b_u$ and $4a_g$ orbital plus 0.30 × curve 1 of the summed $5b_u$ and $5a_g$ orbitals in Fig.7.

5. Summary

In summary, the first measurements of the valence shell binding energy spectra and momentum distributions of the complete valence orbitals of diacetyl by the use of electron momentum spectroscopy are reported. The experimental momentum distributions are compared with the theoretical momentum profiles calculated using HF and DFT/B3LYP methods employing the STO-3G, 6-31G and 6-311++G** basis sets. In comparing the experimental momentum profiles with the calculated distributions, although the experimental profiles could be generally well descried by the calculations when large and diffuse basis sets are used, it also shows that it is difficult to give a good description of the experimental profiles for some

orbitals of large molecules, particularly in the low momentum range (corresponding to the chemically sensitive outer spatial regions of the electron distribution). The pole strengths of the ionization peaks from the inner valence orbitals are also estimated.

References

[1] Amaldi U, Egidi A, Marconero R and Pizzella R 1969 *Rev. Sci. Instrum.* **40** 1001

[2] Weigold E, Hood S T and Teubner O J O 1973 *Phys. Rev. Lett.* **20** 475

[3] McCarthy I E and Weigold E1991 *Rep. Prog. Phys.* **91** 789

[4] Brion C E 1993 *Phys. Elec. At. Coll.* Ed. T. Andersen 1993 AIP press, Proceedings (XVIII ICPEAC), New York 350

[5] Leung K T 1991 *Sci. Progress* Oxford **75** 157

[6] Su G L, Ren X G *et al* 2005 *Acta Phys. Sin.* **54** 4108 (in Chinese)

[7] Zheng Y, Neville J J and Brion C E 1995 *Science* **270** 786

[8] Zhang S F, Su G L *et al* 2005 *Acta Phys. Sin.* **54** 1552 (in Chinese)
Wu X J, Chen X J *et al* 2004 *Chin. Phys.* **13** 1875

[9] Su G L, Ning C G, Zhang S F *et al* 2004 *Chem. Phys. Lett.* **390** 162

[10] Su G L, Ning C G, Zhang S F *et al* 2005 *J. Chem. Phys.* **122** 54301

[11] Neville J J, Zheng Y and Brion C E 1996 *J. Am.Chem. Soc.* **118** 10533

[12] Litvinyuk I V, Zheng Y and Brion C E 2000 *Chem. Phys.* **253** 41

[13] Neville J J, Zheng Y, Hollebone B P, Cann N M, Brion C E, Kim C K and Wolf S 1996 *Can. J. Phys.* **74** 773

[14] Litvinyuk I V, Young J B, Zheng Y, Copper G and Brion C E 2001 *Chem. Phys.* **263** 195

[15] Lanciotti R, Patrignani R, Bagnolini F, Guerzoni M E and Gardini F 2003 *Food Microbiol* **20** 537

[16] Kimura K, Katsumata S, Achiba Y, Yamazaki T and Iwata S 1981 *Handbook of HeI Photoelectron Spectra of Fundamental Organic Molecules* Japan Scientific Society Tokyo p160

[17] Niessen W Von, Bieri G and Åsbrink L L 1980 *J. Electron Spectrosc. Relat. Phenom.* **21** 175

[18] Hernández E J G, Estepa R G and Rivas I R 1995 *Food Chem.* **53** 315

[19] Deng J K, Li G Q, He Y *et al* 2001 *J. Chem. Phys.* **114** 882

[20] Ning C G, Deng J K, Su G L, Zhou H and Ren X G 2004 *Rev. Sci. Instrum.* **75** 3062

[21] Duffy P, Chong D P, Casida M E and Salahub D R 1994 *Phys. Rev.* A **50** 4704

[22] Gaussian 98 (Revision A.6), Frisch M J, Trucks G W, Schlegel H B *et al* Gaussian, Inc., Pittsburgh PA, 1998

[23] Hehre W J, Stewart R F and Pople J A 1969 *J. Chem. Phys.* **51** 2657

[24] Krishnan R, Frisch M J and Pople J A 1980 *J. Chem. Phys.* **72** 4244

[25] Clark T, Chandrasekhar J, Spitznagel G W and Schleyer P V R 1983 *J. Comp. Chem.* **4** 294

[26] Frisch M J, Pople J A and Binkley J S 1984 *J. Chem. Phys.* **80** 3265

[27] Hagen K and Hedberg K 1973 *J. Am. Chem. Soc.* **95** 8266

[28] Duffy P, Casida M E, Brion C E and Chong D P 1992 *Chem. Phys.* **159** 347

[29] Fukui K 1971 *Accounts Chem.* **4** 157

[30] Woodward R B and Hoffman R 1970 *The Conservation of Orbital Symmetry* (Weinheim: Verlag Chemie)

[31] Brion C E, Zheng Y, Rokle J, Neville J J, McCarthy I E and Wang J 1998 *J. Phys.* B **31** L223

[32] Rolke J, Zheng Y, Brion C E, Shi Z, Wolfe S and Davidson E R 1999 *Chem. Phys.* **244** 1

[33] Rolke J, Zheng Y, Brion C E, Chakravorty S J, Davidson E R and McCarthy I E 1997 *Chem. Phys.* **215** 191